Solar light CO_2 photoreduction enhancement by mononuclear rhenium(I) complexes: Characterization and mechanistic insights

*Marcos A. Bento,[1] Nuno A. G. Bandeira,[2] Haralampos N. Miras,[3] Artur J. Moro,[4] João Carlos Lima,[4] Sara Realista,[1] Michael Gleeson,[5] Edwin J. Devid,[5] Paula Brandão,[6] João Rocha,[6] Paulo N. Martinho[1]**

[1] Centro de Química Estrutural, Institute of Molecular Sciences, Departamento de Química e Bioquímica, Faculdade de Ciências, Universidade de Lisboa, Campo Grande, 1749-016 Lisboa, Portugal

[2] Biosystems and Integrative Sciences Institute (BioISI), Departamento de Química e Bioquímica, Faculdade de Ciências Universidade de Lisboa, 8.5.53 - C8 Campo Grande, 1749-016 Lisboa, Portugal

[3] School of Chemistry, The University of Glasgow, Glasgow G12 8QQ, UK

[4] LAQV-REQUIMTE, Department of Chemistry, NOVA School of Sciences and Technology (NOVA-FCT), 2829-516 Caparica, Portugal

[5] Dutch Institute for Fundamental Energy Research (DIFFER), De Zaale 20, 5612 AJ Eindhoven, The Netherlands

[6] Department of Chemistry, CICECO-Aveiro Institute of Materials, University of Aveiro, Portugal

Keywords: CO_2 Photoreduction, metal-based catalysts, solar energy, reaction mechanisms

ABSTRACT

The photocatalytic efficacy of a novel mononuclear rhenium(I) complex in CO_2 reduction is remarkable, with a turnover number (TON_{CO}) of 1517 in three hours, significantly outperforming previous Re(I) catalysts. This complex, synthesized via a substitution reaction on an aromatic ring to form a bromo-bipyridine derivative, **L1** = 2-Bromo-6-(1*H*-pyrazol-1-yl)pyridine, and further reacting with $[Re(CO)_5Cl]$, results in the facial-tricarbonyl complex $[Re\mathbf{L1}(CO)_3Cl]$ (**1**). The light green solid was obtained with an 80% yield and thoroughly characterized using cyclic voltammetry, NMR, FTIR and UV-vis spectroscopy. Cyclic voltammetry under CO_2 atmosphere revealed three distinct redox processes, suggesting the formation of new electroactive compounds. The studies on photoreduction highlighted the ability of the catalyst to reduce CO_2, while NMR, FTIR, and ESI mass spectrometry provided insights into the mechanism, revealing the formation of **solvent-coordinated** complexes and new species under varying conditions. Additionally, computational studies (DFT) were undertaken to better understand the electronic structure and reactivity patterns of **1**, focusing on the role of the ligand, spectroscopic features, and redox behavior. This comprehensive approach provides insights on the intricate dynamics of CO_2 photoreduction, showcasing the potential of Re(I) complexes in catalysis.

INTRODUCTION

Human-induced activities and dependency on fossil fuels have significantly escalated the issue of climate change, primarily through the continuous rise in CO_2 emissions affecting the Earth's thermal balance.[1,2] In tackling this global challenge, researchers are turning towards novel methods such as CO_2 photoreduction, utilizing renewable energy like sunlight to transform CO_2 into useful products such as fuels and chemicals.[3–5]

Metal-based catalysts play a significant role in the process of CO_2 photoreduction, effectively converting it into a diverse range of products such as fuels,[6,7] sustainable materials,[8] and essential chemical feedstocks.[9-11] These catalytic systems are typically composed of multiple components, one of which is a redox photosensitizer that triggers electron transfer from a sacrificial donor to the catalyst, ultimately transferring these electrons to the CO_2 molecule. The advantage of these systems lies in their flexibility, allowing for the adjustment of each component (photosensitizer and sacrificial donor) individually to enhance the efficiency of the catalyst. However, the electron transfer process between the different components is limited and hampered, primarily due to diffusion-collision.[12,13]

One solution to overcome these limitations in CO_2 photoreduction is the use of photocatalysts. Among the notable compounds in this field are Re(I) bipyridine complexes, which have been a subject of study since their introduction by Lehn and Hawecker in 1980.[14] Recent research has unveiled various mononuclear and binuclear rhenium complexes inspired by this pioneering work, resulting in increased efficiency and durability. Nevertheless, challenges remain, such as the energy input required, the quantity of catalyst needed, and the reliance on high-power visible light lamps for photocatalyst activation. For example, *fac*-[Re(pyr)$(CO)_3$Cl] and *fac*-[Re(bpy)$(CO)_3$Cl] were studied as catalysts for CO_2 photoreduction into CO in DMF/TEOA (5:1) solutions with

concentrations around the millimolar range (1 and 0.026 mM, respectively) and a 300 W Xe lamp (equipped with a 350 nm cutoff filter) exhibiting a good photocatalytic activity and stability (TON_{CO} = 120 and TON_{CO} = 17, respectively).[14–21]

To address these challenges and enhance the photocatalytic activity and durability of rhenium photocatalysts, researchers have employed a ligand functionalization approach using photoactive units, such as π-conjugated aromatic groups with electron-donating and electron-withdrawing groups.[18, 22-24] Recognizing the significant role played by the ligand in the photoreduction of CO_2, our objective is to develop a new family of rhenium photocatalysts with superior activity for CO_2 photoreduction. To achieve this, we have initiated the development of a versatile ligand for functionalization and have prepared a novel Re(I) complex that serves as an active and selective photocatalyst for CO_2 conversion, operating efficiently even at concentrations as low as nanomolar levels.[14, 24–32]

EXPERIMENTAL SECTION

General remarks

All reagents were used without further purification. The reagents used were purchased from different companies such as Sigma Aldrich, Acros Organics, Fluorochem and/or TCI. Solvent purifications were performed according to the book "Purification of Laboratory Chemicals" by Armarego and Perrin.[33] All reactions were done using standard Schlenck techniques and freshly distilled solvents. NMR spectra were recorded on a Bruker Advance 400 spectrometer using deuterated solvents (dimethylsulfoxide-d_6 (DMSO-d_6), dimethylformamide-d_7 (DMF-d_7), CD_3CN, CD_2Cl_2). FTIR spectra were obtained on a Nicolet 6700 FTIR spectrophotometer in the 400-4000 cm^{-1} range with 4 cm^{-1} resolution using KBr pellets. Elemental analysis (EA) for C, H

and N were performed with a Truspec Micro CHNS 630 200 200 elemental analyser at the Department of Chemistry, University of Aveiro. Analysis parameters: sample amount 1.3 - 2.0 mg; combustion furnace temperature 1075 ºC; afterburner temperature 850 ºC. Detection method: C, H and S through infrared absorption; N by thermal conductivity. Gases required: combustion - oxygen; carrier helium; pneumatic - compressed air.

All MS data were collected using a Q-trap, time-of-flight MS (Maxis Impact MS) instrument supplied by Bruker Daltonics Ltd. The detector was a Time-of-Flight, micro-channel plate detector and all data were processed using the Bruker Daltonics Data Analysis 4.1 software, whilst simulated isotope patterns were investigated using Bruker Isotope Pattern software and Molecular Weight Calculator 6.45. The calibration solution used was Agilent ES tuning mix solution, Recorder No. G2421A, enabling calibration between approximately 100 m/z and 2000 m/z. This solution was diluted 60:1 with MeCN. Samples were dissolved in DMF/MeOH (2:1) and introduced into the MS via direct injection at 180 μL h^{-1}. The ion polarity for all MS scans recorded was positive, at 180 ºC, with the voltage of the capillary tip set at 4000 V, endplate offset at –500 V, funnel 1 RF at 300 Vpp and funnel 2 RF at 400 Vpp.

Synthesis

2-Bromo-6-(1H-pyrazol-1-yl)pyridine (**L1**) was synthesized according to a literature method.[34]

[Re**L1**$(CO)_3$Cl] (**1**)

To a solution of **L1** (224.6 mg, 1.002 mmol) in toluene (20 mL) was added rhenium pentacarbonyl chloride (361.7 mg, 1.000 mmol) and this solution was mixed for 17 h at 110 ºC. During this time, a light green solid formed. Afterward, the reaction mixture gradually cooled to

room temperature. The solution was then concentrated, and the solid was separated by filtration, washed with diethyl ether (3 × 10 mL) and tetrahydrofuran (1 × 10 mL, THF). The resulting solid was dried under vacuum for 6 hours, yielding 424 mg of the final product (yield: 80%). Crystals suitable for single crystal X-ray diffraction (SCXRD) analysis were obtained by layering a solution of the complex in dichloromethane with diethyl ether. ^{1}H NMR (400 MHz, DMF-d_7, 298 K): δ = 9.35 (d, J = 3.0 Hz, ^{1}H), 8.63-8.50 (m, 2H), 8.35 (t, J = 8.1 Hz, ^{1}H), 8.13 (d, J = 7.8 Hz, ^{1}H), 7.07 – 7.01 (m, ^{1}H); ^{13}C NMR (100 MHz, DMF-d_7, 298 K): δ = 199.22, 197.07, 191.30, 147.37, 144.90, 140.59, 133.89, 113.30, 129.62, 113.16; UV-vis (nm, DMF): 349, 355; FTIR (cm^{-1}, KBr pellets): ṽ(C-H): 3097 cm^{-1}, ṽ(CO): 2028, 1927, 1911 cm^{-1}, ṽ(C=C): 1600 and 1470 cm^{-1}, ṽ(C=N): 1568; Elemental Analysis for [Re($C_8N_3H_6Br$)$(CO)_3$Cl]: exp. C 24.6, H 1.1, N 8.1 calc. C 24.8, H 1.7, N 7.9.

Crystallography

Crystals suitable for SCXRD analysis were grown as described in the synthetic procedures and the data was collected at 150(2) K using a RIGAKU XtaLAB Synergy-i equipped with a Mo Kα (λ = 0.71073 Å) PhotonJet-i microsource, a HyPix3000 detector controlled by the CrysAlisPro software (Y. Oxford Diffraction Ltd, England, 2022, CrysAlis PRO, Rigaku V1.171.142.173a) and equipped with an Oxford Cryosystems Series 800 cryostream. Diffraction images were processed using the CrysAlisPro software and data was corrected for absorption by the multi-scan absorption correction using spherical harmonics implemented in SCALE3 ABSPACK scaling algorithm. The structures were solved by the direct methods using SHELXT 2014/5 and refined by weighted full matrix least-squares method on F2 using SHELXL2018/3.[35] All non-hydrogen

atoms were refined with anisotropic thermal parameters. Molecular diagrams were drawn with Mercury software.[36] The data for **1** was deposited in CCDC under the deposit numbers 2327449.

Photoreduction experiments

CO_2 photoreduction experiments were performed in a 16 mL quartz reactor, directly exposed to low-voltage solar lamp irradiation (Philips, Projection lamp type 13117, 18.82 V, 160 W). The experiments were carried out under a saturated CO_2 atmosphere using 5 mL solutions of different concentrations of the catalyst (0.25 mM, 2.5 mM, 25 mM, 250 mM, 500 mM and 1000 mM), TEOA (0.3 M) in DMF. These solutions were stirred with a magnetic bar and irradiated for several periods of time at 60 ºC (residual heating from the light source). The gases produced were analyzed by gas chromatography equipment fitted with a thermal conductivity detector (GC-TCD) using gas-tight syringes (500 µL) previously purged with CO_2 and the liquid products were not analyzed. Following each injection, the temperature of the quartz reactor was measured using a thermometer.

For gaseous products quantification, was GC-TCD used from Agilent Technology (GC-TCD 7820A) controlled by OpenLAB ChemStation edition software. A HP-MOLESIEVE capillary GC Column (L×I.D. 30 m×0.32 mm, average thickness 12 µm) was used for H_2, CO, CH_4 and CO_2 detection. The temperature was held at 200 ºC and 220 ºC both for the injector and the detector (respectively). The carrier gas was Ar flowing at 1.7 mL min^{-1} and injections were performed with gas-tight syringes (250 or 500 µL) previously purged with CO_2. The method was based on a temperature ramp in the oven starting at 40 ºC for 8 min and gradually increased to 200 ºC for 12 min (retention times (min): H_2 1.91, O_2 2.14, N_2 2.62, CH_4 3.17, CO 5.94, CO_2 13.18). Calibration curves were obtained for H_2, CO and CH_4 separately by injecting known volumes of the pure gas.

Electrochemistry

Cyclic voltammetry experiments were performed using 1 mM DMF solutions of the complex, under N_2 or CO_2 saturated atmosphere in a three-electrode one compartment electrochemical cell at 0.1 mV s^{-1}. Glassy carbon (CHI Instruments, 3 mm diameter) and platinum wire were used as working and counter electrodes, respectively. Ag wire was used as the pseudo-reference electrode and tetrabutylammonium hexafluorophosphate ($TBAPF_6$) as the supporting electrolyte (recrystallized from hot ethanol). Ferrocene was used as an internal standard and all potentials are referenced to ferrocene/ferrocenium couple. The working electrode was polished with alumina paste of 1 and 0.05 μm diameter sizes and washed thoroughly with Milli-Q water and dried under a nitrogen flux.

Fluorescence and UV-vis studies

UV-vis spectra were recorded on a Shimadzu 50/60 Hz spectrometer using a 3 mL solution of **1** (5×10^{-5} M) in the desired solvent (DMF or DCM). The time dependent experiments were performed using the same solution of **1** in DMF until no changes in the spectrum were observed. Emission spectra were recorded on a Horiba-Jobin-Yvon SPEX Fluorolog 3.22 spectrofluorometer.

Electrospray Ionization Mass spectrometry (ESI-MS) solution studies

The ESI-MS studies were performed in DMF:MeOH (2:1) solution in positive ionization mode. During the course of the CO_2 photoreduction experiments a 0.3 M TEOA solution in DMF saturated with CO_2 containing an amount of **1** (0.25 mM) was used. Subsequently, the solution was irradiated in a quartz cell using a low voltage halogen lamp (100 W) for 4 hours.

Computational Methods

Electronic structure calculations performed made use of the ORCA version 5.0.4 software[37] package throughout. The hybrid PBE0 density functional[38,39] was used (also known as PBE1PBE) in conjunction with Grimme's D4 correction[40].

The triple-zeta relativistic all electron x2c-SVP basis sets[41] was used for the light elements and x2c-TZVP for rhenium. The IORA modified metric relativistic Hamiltonian[42] (IORAmm) was used.

The Resolution of Identity with the Chain of Spheres approximation[43,44] (RIJCOSX) was used in the multi-centre integral solving with the default integration grid settings and corresponding auxiliary basis set (x2c/J). Implicit solvation effects were modelled by the Conductor-like Polarizable Continuum Model[45,46] (CPCM) with default settings for dimethylformamide.

Analytic Hessian analysis was carried out on all obtained stationary points to confirm their nature. Transition states underwent re-optimization with a fractional displacement of the imaginary vibrational mode to confirm the reaction pathway in both directions. Free Energies were computed for a temperature of 298.15 K.

To avoid any charge artifacts the **A**→**B** transformation was calculated as the direct free energy difference between the [Re**L1**$(CO)_3$(DMF)]$^+$…Cl^- ion pair and the [Re**L1**$(CO)_3$Cl]…DMF van der Waals pair.

The standard reduction potentials are reported against ferrocenium (Fc^+)/ferrocene (Fc) pair as the reference. The calculated absolute potential at the chosen level of theory was $E_{abs}(Fc^+/Fc)$=+5.182 eV. The calculated redox potentials were therefore estimated as follows: $E^{\ominus} = -(G_{red}-G_{ox}) - E_{abs}(Fc^+/Fc) = -\Delta G - 5.182$ V.

Intra-fragment charge transfer (IFCT) analyses were estimated using the protocol implemented in the MultiWfn software program[47] version 3.8 with Hirshfeld charge fragment partitioning.

Emission spectra was simulated using ORCA's ESD module[48] employing both the calculated ground and excited state Hessians. Time-Dependent DFT optimizations were carried out for the target root among a selection of 40 scalar (singlet and triplet) states equivalent to 160 SOC states.

RESULTS AND DISCUSSION

Synthesis and characterization

L1 was synthesized using a well-established method, described in the literature.[34] This synthesis involved a substitution reaction on an aromatic ring to generate a bromo-bipyridine derivative. This compound was then used as a ligand in the preparation of the rhenium(I) complex. The process entailed mixing **L1** with $[Re(CO)_5Cl]$ in toluene, followed by refluxing the mixture for 17 hours. This procedure successfully yielded the anticipated facial-tricarbonyl complex (**1**), which was obtained in a light green solid form. The synthesis was notably efficient, achieving an 80% yield.

Single crystals of **1** were successfully grown employing a layering technique. This involved carefully overlaying a dichloromethane solution of **1** with diethyl ether, which promoted the formation of well-defined crystals suitable for X-ray analysis. To characterize **1**, various analytical techniques were employed, including ^{1}H and ^{13}C NMR, FTIR, elemental analysis, UV-vis spectroscopy, photoluminescence, and cyclic voltammetry.

The compound displayed six ^{1}H NMR aromatic resonances assigned to the coordinated ligand. ^{13}C and HSQC NMR allowed the unambiguous assignment of the carbon and carbonyl resonances

of **1** (Figures S1-S4). FTIR confirmed the presence of the characteristic vibrational modes of carbonyl groups $\tilde{\nu}$(C=O) at 2028, 1927, and 1911 cm^{-1}, as well as the bands attributed to pyridine, imidazole, and aliphatic groups at $\tilde{\nu}$(C-H) at ~3000 cm^{-1}, $\tilde{\nu}$(C=C) and $\tilde{\nu}$(C=N) between ~1400 and 1600 cm^{-1}. The $[Re(CO)_5Cl]$ precursor was not detected by FTIR (Figure S5).

This mononuclear rhenium complex crystallized in the triclinic space group $P\bar{1}$. The complex exhibits a facial octahedral geometry, with the ligand coordinating to the metal center in the equatorial plane (Figures 1 and S6). The angle between the ligand and the rhenium metal center is 73.86º resulting in a complex with a distorted octahedral geometry (Tables S1 and S2). A comparison between the powder X-ray diffraction pattern of the synthesized sample and the simulated pattern derived from single crystal data reveals that the crystals obtained are representative of the bulk sample (Figure S7).

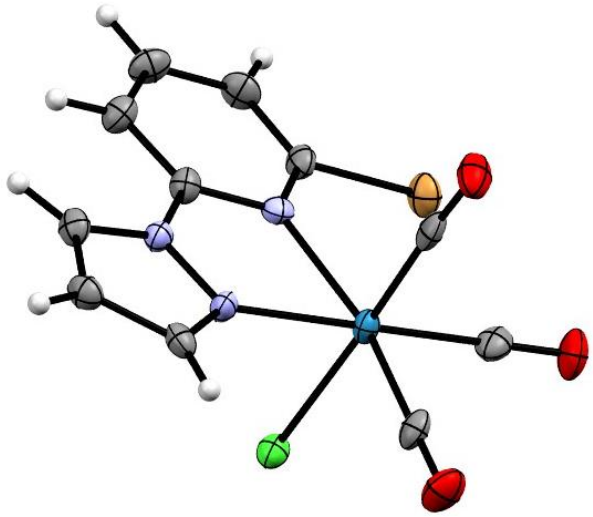

Figure 1: ORTEP diagram of the X-ray crystal structure of **1** with thermal ellipsoids at the 50% probability level. Re (dark blue); Br (brown); Cl (green); O (red); N (blue); C (grey); H (white).

The structure of **1** was optimized in the ground state with the PBE0-D4 density functional. The optimized bond lengths are slightly underestimated with respect to the experimental values (Table S3) but the agreement is excellent.

The nature of the electronic structure is typical of what is expected of a $5d^6$ octahedral complex. There is a sizable HOMO-LUMO gap (4.14 eV) and the first two virtual MOs (LUMO and LUMO+1) are mostly ligand centered (Figure S8).

The formation of **solvent-coordinated** complexes is frequently observed in facial tricarbonyl rhenium(I) complexes when coordinating solvents are present [22,49–53], and the compound in question is no exception. The formation of these solvated compounds was confirmed by ^{1}H and ^{13}C NMR using CD_3CN, DMSO-d_6 and DMF-d_7, as well as the non-coordinating solvent CD_2Cl_2 (Figures S9-S12) and evidenced as well as by mass spectrometry studies.

The ^{1}H NMR spectra in the coordinating solvents verified the presence of a **solvent-coordinated** species, as evidenced by the emergence of new peaks, some of which overlapped with the original compound. Notably, the ratio of the initial complex to the **solvent-coordinated** complex stands at 2:1 for DMSO-d_6 and DMF-d_7 and 1:1 for CD_3CN after 72 h, suggesting a greater exchange for the latter. No new peaks appeared in CD_2Cl_2, further supporting the formation of **solvent-coordinated** compounds in the presence of coordinating solvents. The HSQC NMR spectrum unequivocally assigned the signals from **1** and the **solvent-coordinated** complex (Figure S4).

The behavior of **1** in solution was further analyzed by UV-vis spectroscopy and the results were compared with those obtained computationally. The UV-vis spectrum of **1** exhibits a π-π* intra-ligand band, and a low energy metal-ligand charge transfer (MLCT), possibly $d\pi_{Re}$-π_{NN}*, at 307 nm and 355 nm, respectively. This assignment is borne out by computational analysis. It is clear that a metal-ligand charge transfer (MLCT) character occurs among the first electronic transitions.

Indeed, the character of the Frank-Condon electronic transitions can be assigned upon performing a time-dependent calculation. The agreement with the experimental spectrum is good with regards to the most intense band showing up at 292 nm (Figure 2). The theoretical prediction is at 274 nm. However, in the calculated spectrum a weak transition also emerges at 359 nm, and this is likely the weak shoulder visible at 318 nm. While the agreement with experiment is only fair in this instance it is quite reasonable.

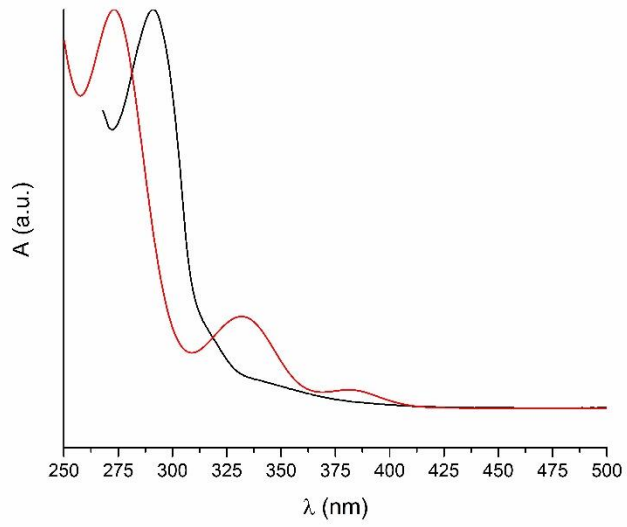

Figure 2: Normalized experimental (black) and calculated (red) absorption spectrum of **1**.

The first (weak) band corresponds to an MLCT and is attributable to the second excited state singlet (S_2) and is a HOMO-1→LUMO transition. The most intense absorption band corresponds to two quasi-degenerate transitions S_8 and S_9, the latter contains a majority HOMO-3→LUMO character with a minor contribution of 29% HOMO-2→LUMO+1. HOMO-3→LUMO is a majority intra-ligand transition (Table S4 and Figure S13).The formation of the **solvent-coordinated** complex was also followed by UV-vis spectroscopy. After 72 h, **1** partially transformed into the **solvent-coordinated** form in DMF, as evidenced by the emergence of two

distinct bands at 290 nm and 320 nm (Figures S14 and S15, and Table S5). To explore the influence of light on the creation of this **solvent-coordinated** entity, a DMF solution of **1** was exposed to light for 3 hours and subsequently analyzed using UV-vis spectroscopy. This revealed the development of a novel compound characterized by absorption bands at 307 nm and 355 nm. Interestingly, this spectral signature mirrors that of the **solvent-coordinated** complex formed after 72 hours, suggesting that light speeds up the transformation of **1** into its **solvent-coordinated** species. The emission spectrum of the sample after 72 h at 300 K presents an emission band with a maximum centered at 330 nm, while at 77 K a stronger emission band at 410 nm appears (Figure S16). This temperature dependence suggests that this latter emissive band is associated with a ^{3}MLCT transition, as previously observed for similar Re complexes.[54]

Computational studies revealed that upon the introduction of spin-orbit coupling (SOC) via the spin-orbit mean field (SOMF)[55] approach the character of the second band becomes more convoluted. Scalar roots S_8 and S_9 are quasi-degenerate and exhibit oscillator strength values of 0.128 and 0.342, respectively. SOC of these lead to spinor roots 44 and 45, with oscillator strengths 0.151 and 0.240 respectively, both heavily admixed with the 13th triplet (T_{13}).

Since the electronic states of the second band have a diverse make-up an intra-fragment charge transfer analysis was performed on two fragments: {$Re(CO)_3Cl$} and **L1**. These will provide the net electron gain by the ligand from the metallic fragment. While the first band is assuredly an MLCT transition, the second one has more limited MLCT character as may be seen from Table S3.

To describe the photon emission process, a geometry optimization was also performed on one of the highest absorbing SOC states, i.e., root 44. The relaxed geometry is not substantially different from that of the ground state, the largest deviation being the ring bridge N(2)-C(8) which

contracts its bond length by 2.3 pm. There is also a shortening of the Re-N(1) bond by 1.8 pm and an enlargement of the Re-N(3) one by 1.3 pm.

The calculated emission spectrum is close to the experimental one (Figure 3). The experimental band maximum is at 330 nm and the calculated one is at 314 nm. The final composition of the spinor state is $61\%S_8+22\%T_{13}$ where each of the transition densities is identical to those shown in Figure 2. The estimated MLCT fragment character of this spinor state is $0.03e^-$ which makes it a majority intra-ligand transition as opposed to the usual MLCT in complexes of this type.

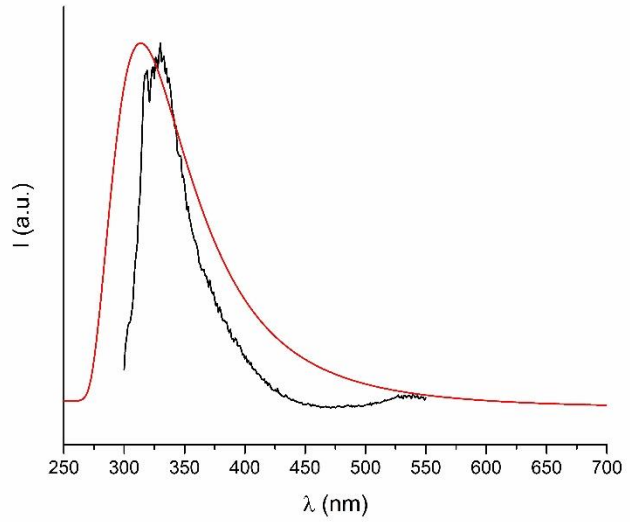

Figure 3: Normalized calculated (298 K, red) versus experimental (300 K) emission spectrum of **1** (5×10^{-5} M) in DMF (λ_{exc}=290 nm).

Redox behavior

The cyclic voltammograms of **1** were recorded in DMF using 0.1 M $TBAPF_6$ electrolyte under N_2 atmosphere (Figure S18). The complex displays three reduction events at -1.26, -1.73 and -2.13

V *vs*. Fc/Fc^+ and three oxidation processes at -0.33, -0.46 and -2.08 V *vs*. Fc/Fc^+. The first reduction (-1.73 V *vs*. Fc/Fc^+) is ascribed to a one-electron reduction of the ligand $NN/NN^{\bullet-}$.[17] The second reduction (-2.14 V *vs*. Fc/Fc^+) is attributed to a second one-electron reduction of the ligand. The remaining redox events are due to other ligand processes.[56–60]

The redox potentials for complexes **1** and **solvent-coordinated**, were calculated referenced to the ferrocenium/ferrocene couple, considering both their ground and excited states and compared with the the experimental ones obtained with cyclic voltammetry. It was found that the reduced species is not a formal Re(0) complex but rather an organic-based radical. This conclusion is supported by the characteristics of the singly occupied molecular orbitals (SOMOs), as shown in Figure 4, and the Löwdin spin densities observed on the metal fragments, which are 0.00 for complex **1** and 0.019 for complex **solvent-coordinated**, respectively.

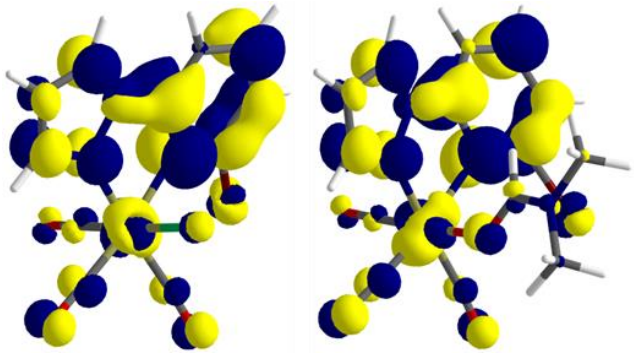

Figure 4: SOMOs (Unrestricted Natural Orbitals) of the $1e^-$ reduced species **1** (left) and the analogous **solvent-coordinated** complex (right).

Photoreduction studies

In the past few years, multiple research teams have delved into the study of both mononuclear and binuclear rhenium complexes under the influence of visible light irradiation in a DMF/TEOA mixture.[14] Taking inspiration from these studies on rhenium complexes and the corresponding

characterization data, we assessed our compound during a series of CO_2 photoreduction experiments. For these experiments, we employed **1** as the catalyst in a CO_2-saturated DMF environment in the presence of TEOA (0.3 M). We subjected the solution to visible light irradiation using a solar simulator. To improve the CO_2 photoreduction efficacy of this mononuclear rhenium complex, we performed several optimization trials and control experiments. The catalyst preferentially yielded 1.90 μmol of CO, achieving a TON_{CO} of 1517 within a span of 3 hours at 60 ºC, with a ϕ_{CO} of 0.03 % (Table 1, Figures S19 and S20). The experiments were conducted at 60 ºC, a decision driven by the localized temperature spike from the lamp's irradiation. Remarkably, our catalyst's TON_{CO} values surpass those of the best Re(I) catalysts previously reported for CO_2 photoreduction under similar conditions. In our experiments, we used catalyst concentrations ranging from 0.25 to 1.000 μM, and our reaction durations were consistently under 3 hours. This contrasts with the earlier Re(I) catalysts, which typically required much higher concentrations (in the millimolar range) and considerably longer reaction times, often exceeding 24 hours. Some of the most promising catalysts reported are *fac*-[Re(pyr)$(CO)_3$Cl] (TON_{CO} = 125, DMF/TEOA(5:1), after 24 h) where pyr = 4,7-bis(1*H*-pyrrole-1-yl)-1,10-phenanthroline, *fac*-[Re(pypyri)$(CO)_3$Cl], where pypyri = 9-(pyren-1-yl)-10-(pyridin-2-yl)-9*H*-pyreno[4,5-*d*]imidazole, (TON_{CO} = 124, DMF/TEOA (5:1), BIH (20 mM), after 8 h) and *fac*-[Re(BDP_2)$(CO)_3$Cl], where BDP_2 = 4,4'-bis(4-(5,5-difluoro-1,3,7,9-tetramethyl-5*H*-4 |4,5 |4-dipyrrolo[1,2-*c*:2',1'-*f*][1,3,2]diazaborinin-10-yl)phenyl)-2,2'-bipyridine, (TON_{CO} = 1320, DMF/TEOA (5:1), BIH (140 mM), after 30 h).[22,31,62]

Table 1: Optimization of the catalyst concentration for the CO_2 photoreduction reaction.

Entry	[Cat] [μM]	n_{H_2} [μmol]	n_{CO} [μmol]	Selectivity$_{CO}$ [%]	TON$_{CO}$	TOF$_{CO}$ [h^{-1}]	Φ [%]
1	0	tr.	0.70	-	-	-	-
2	0.25	tr.	1.90	>99	1517	506	0.03
3	2.5	tr.	1.46	>99	117	39	0.03
4	25	tr.	2.02	>99	16	5	0.04
5	250	tr.	3.33	>99	3	1	0.06
6	500	tr.	2.56	>99	1	0.3	0.05
7	1000	tr.	4.11	>99	1	0.3	0.07

Reaction conditions: 5 mL DMF, TEOA (0.3 M), visible light (Philips, Projection lamp type 13117, 18.82 V, 160 W), 3 h experiment, 6.26×10^{17} photons per second calculated for this apparatus by using $K_3[Fe(C_2O_4)_3]$ actinometer. tr. = traces

During the series of conducted control experiments under a N_2 atmosphere, it was confirmed that the main source of CO production was the photoreduction of CO_2 by **1**. (Table S6, Figures S21-S23) We have found that in blank experiments, the CO generation process is primarily influenced by the light intensity and the inherent temperature surge due to lamp exposure. Interestingly, using a non-coordinating solvent like dichloroethane (DCE) revealed that **1** is not catalytically active during the CO_2 photoconversion process. This highlights the essential coordination role of DMF coordination in this reaction, as presented in Table S6. Additionally, studies employing a 72-hour DMF solution of **1** revealed that the presence of **solvent-coordinated** complexes does not inhibit the conversion. This suggests that the transformation of **1** into its **solvent-coordinated** variant is a pivotal initial step in the CO_2 photoreduction mechanism.

To study the performance of **1** as function of time, we conducted a series of experiments using a range of exposure times, ranging from 1 to 6 hours. (Table S7, Figures S24 and S25) Notably, the catalyst reaches maximum conversion after a 3-hour interval, registering a TON of 1517 and a

TOF of 506 h^{-1}. Conversely, after 1 hour, the catalyst's CO production is equal to the blank experiment. This observation suggests that an induction time interval is needed before the catalyst becomes fully operational. However, after the 6-hour threshold, there was a considerable decrease in the catalyst activity. This decrease suggests that potential simultaneous processes take place, such as catalyst degradation, dimerization of the active entities, or the synthesis of rhenium TEOA−CO_x adducts (where x = 0 or 2) that can sequester either the generated CO or the dissolved CO_2.[12,32,52,53,63]

Mechanistic investigation

To get insight into the mechanism driving the interaction with CO_2, and to discern the formation of novel compounds under varying conditions (whether in different solvents, under light exposure, or in the presence of SDs) we employed analytical techniques including FTIR and ESI mass spectrometry. The FTIR spectra exhibits two new peaks at 1969 and 2052 cm^{-1} attributed to the **solvent-coordinated** complex. (Figure S26) The mass traces acquired in DMF and DMF/TEOA (5:1) show two peaks at m/z = 800.14 and 873.19 assigned to $\{Re^{0}(CO)_3(C_8N_3H_6Br)(DMF)_3(MeOH)(H_2O)H\}^+$ and $\{Re^{I}(CO)_3(C_8N_3HBr)(DMF)_2(MeOH)_5(H_2O)_3\}^+$, confirming the formation of the **solvent-coordinated** complex discussed in the previous sections (Figure S27, Figure 7 (**B**)).[52,57,61]

The new species detected by the experimental methods prompted us additionally to explore computationally some of the chemical changes that drive the CO_2 reduction forward. Concerning the **A**→**B** transformation (i.e. [Re**L1**$(CO)_3$Cl] + DMF → [Re**L1**$(CO)_3$(DMF)]$^+$ + Cl^-) this was

calculated to be endergonic with a free energy change of +10.8 kcal mol^{-1}. This is consistent with a minute formation of **B** in solution.

The redox behavior of **1**, was also studied under a CO_2 atmosphere, displaying notable changes. Specifically, the initial reduction peak exhibited a shift of -90 mV *vs*. Fc/Fc^+, paired with an increase in cathodic current. Concurrently, there was an enhanced cathodic current observed for the peak at -2.13 V *vs*. Fc/Fc^+, and a new peak emerged at -2.34 V *vs*. Fc/Fc^+, which was attributed to the formation of a new electroactive compound (Figure S18 and Figure S28). [52,61]

These studies were further complemented by cyclic voltammetry experiments conducted under light irradiation and in the presence of TEOA under both N_2 and CO_2 atmospheres. When cyclic voltammetry was undertaken under an N_2 atmosphere with TEOA (0.3 M) present, there was a noticeable decline in the first reduction peak at -1.76 V *vs*. Fc/Fc^+ after 15 minutes of light exposure. This behavior suggests that TEOA is facilitating the reduction of the complex into a one-electron reduced species. Shifting to a CO_2 atmosphere, the cyclic voltammetry behavior of the complex in the presence of TEOA exhibited the vanishing of the first reduction peak at -1.76 V *vs*. Fc/Fc^+ post 30 minutes of irradiation, indicating that the TEOA is reducing the complex under light irradiation. These observations hint at the potential formation of a two-electron reduced species, which could then participate in CO_2 reduction. (Figures S29 to S33) This species appears to be more prevalent in a CO_2 atmosphere when TEOA is present (Figures 5 and 7 (**C**)).[22,57–60,73,74]

The rationale behind the reduction of CO_2 occurring only when a significant population of excited states is present in the solution can be elucidated by examining the calculated reduction potential values in both the ground state and the two categories of excited states previously described (Table 2). The oxidation potential of triethanolamine in a DMF solution, determined experimentally, is +0.37 V. When this value is added to the ground state reduction potentials of

complexes **1** and **solvent-coordinated complex**, the resulting global reduction potential is still significantly negative (unfavorable).

Table 2: PBE0-D4 calculated reduction potentials for species **1** and the **solvent-coordinated complex**.

Reduction potential vs Fc/Fc^+	**1**	**solvent-coordinated**
$E(0e^-/1e^-)$/V	-2.36	-2.17
$E(0e^-*/1e^-)$/V – *MLCT (1st band)	+0.69	+1.77
$E(0e^-*/1e^-)$/V – *ILCT (2nd band)	+2.10	+2.26

Upon forming the first highly absorbing excited states in **1** (SOC root 8) and **solvent-coordinated** (SOC root 11), the reduction potentials become large enough to yield an overall positive reduction potential (second row of Table 2). The next highly absorbing set of excited states in **1** (SOC root 44) and **solvent-coordinated** (SOC root 44) will result in even higher reduction potential values (noted as intra-ligand charge transfer ILCT in the last row of Table 2). Regardless of the nature of the excited state the DMF adduct is the thermodynamically more favorable species to react with the sacrificial electron donor TEOA.

To understand the catalytic system and uncover valuable information about the mechanism, we investigate the composition of the catalytic mixture in solution. Employing high-resolution ESI-MS, we were able to identify stable species that might be crucial to our understanding of the catalytic mechanism within the range of ca. 600 – 1000 m/z.[64,65] These species can be associated back to two plausible reaction pathways: protonation and disproportion of CO_2.[66,67] More specifically the isotopic distribution envelopes centered at 621.94 and 637.95 m/z can be assigned

to the $\{Re^{I}(CO)_3(C_8N_3H_4Br)(DMF)(COOH)\}^+$ and $\{Re^{II}(CO)_3(C_8N_3H_4Br)(DMF)(HCO_3)\}^+$ cations resulting from the reduction of the CO_2 species present in solution. Envelopes centered at 683.03 and 714.00 m/z can be attributed to $\{Re^{I}(CO)_3(C_8N_3H_4Br)(DMF)(MeOH)(H_2O)_4\}^+$ and $\{Re^{I}(CO)_3(C_8N_3H_5Br)(DMF)_2\ (MeOH)_2(H_2O)_4\}^+$ which can be attributed to **1** with different combination of counterions and solvent molecules (Figure 7). Given our current dataset, we propose a CO_2 photoreduction mechanism anchored on CO_2 protonation, taking into account that the residual amount of H_2O in the solvent and TEOA are responsible for donating protons to the system. This preference stems from the limited experimental data available on the formation of the pivotal intermediate species inherent in the CO_2 disproportion mechanism. (Figure 7) [18,40,47,74]

Our studies have led to the identification of the reported TEOA−CO_2 adduct, specifically *fac*-[Re(**L1**)$(CO)_3(CO_2{-}OCH_2CH_2NR_2)$] (R = CH_2CH_2OH). In the range of 800 – 1000 m/z, another group of envelopes has been identified and assigned as a singly charged mononuclear complex with different coordination environment where the sacrificial TEOA moiety is directly involved in this case. More specifically, there are three species with isotopic envelopes centered at 839.10, 867.09 and 911.14 m/z that can be attributed to the $\{Re^{I}(CO)_3(C_8N_3H_5Br)[N(CH_2CH_2OH)_2(CH_2CH_2CO_2)](DMF)_2\}^+$, $\{Re^{II}(CO)_3(C_8N_3H_6Br)[N(CH_2CH_2OH)_2(CH_2CH_2OCO_2)](DMF)(MeOH)_3\}^+$ and $\{Re^{I}(CO)_3(C_8N_3H_5Br)[N(CH_2CH_2OH)_2(CH_2CH_2OCO_2)](DMF)_2(H_2O)_3H\}^+$, respectively.[69-72] These species, with isotopic envelopes centered at 867.09 and 911.14 m/z, is the product of the sequential replacement of the axial DMF ligand by a deprotonated TEOA, followed by the insertion of CO_2 into the Re−O bond (Figure 5 and Figure 7 (species **H** and **I**)).[51,70] Moreover, the discovery of a previously undocumented TEOA−CO adduct, *fac*-[Re(**L1**)$(CO)_3(CO{-}OCH_2CH_2NR_2)$] (R = CH_2CH_2OH), was notable with its isotopic envelope centered at 839.10 m/z. This species is presumably formed

via the nucleophilic attack by a TEOA molecule on the C≡O bond (Figure 5 and Figure 7 (**G**)). The synthesis of these CO_x-TEOA adducts, where x can be either 0 or 2, is in good agreement with the IR analyses conducted in a DMF/TEOA (5:1) mixture. These studies pinpoint the emergence of intermediary species attributed to [Re(**L1**)$(CO)_3$(TEOA)], evidenced by their vibrational frequencies at 2015, 1891, and 1880 cm^{-1} (Figures 5 and 7 (**H**) and Figures S34 and S35).

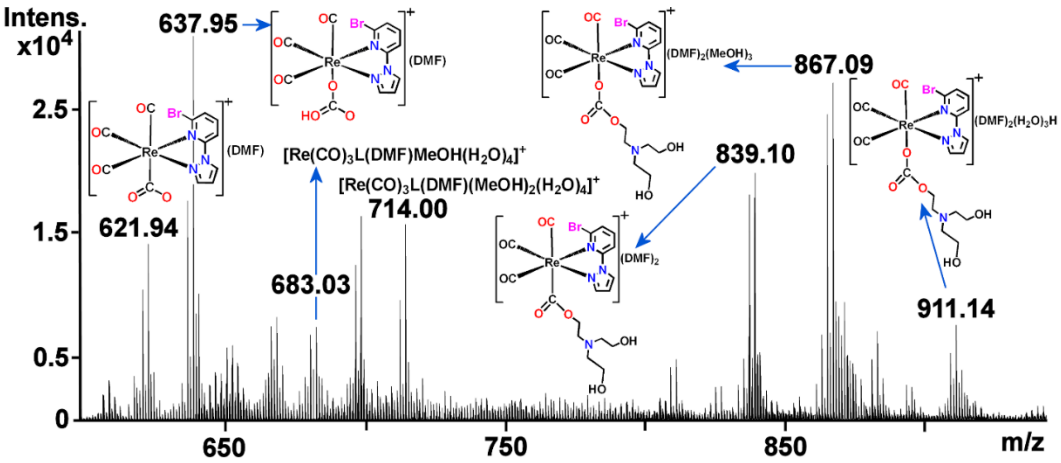

Figure 5: Positive ion ESI mass spectrum of **1** after 4 h of irradiation.

Concerning the **H**→**I** transformation this side reaction was analyzed, and its potential energy profile calculated (Figure S36). While there is an identifiable transition state ($TS1^{‡}$) with 0.7 kcal mol^{-1} activation energy there is also a sizeable (16.8 kcal mol^{-1}) barrier height ($TS2^{‡}$) however for the ligating atom switch within the rhenium coordination sphere. A different picture emerges upon analysis of the **F**→**G** profile (Figure 6). The activation energy is still low but the product lands on a thermodynamic sink and the resulting side product is irreversibly formed with a resulting free energy of -29.0 kcal mol^{-1}.

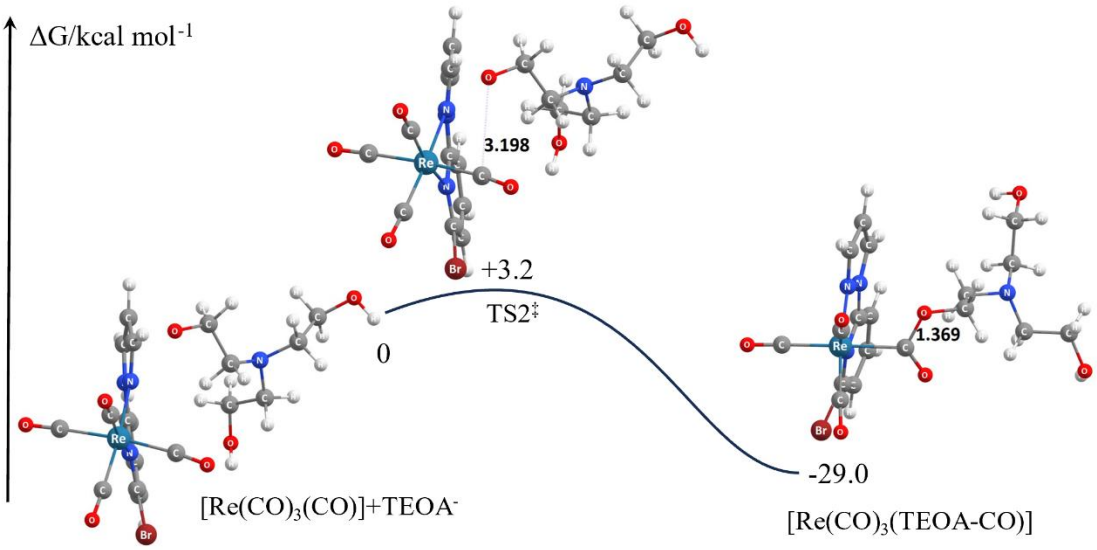

Figure 6: Potential energy profile of the nucleophilic addition of species **F** with TEOA.

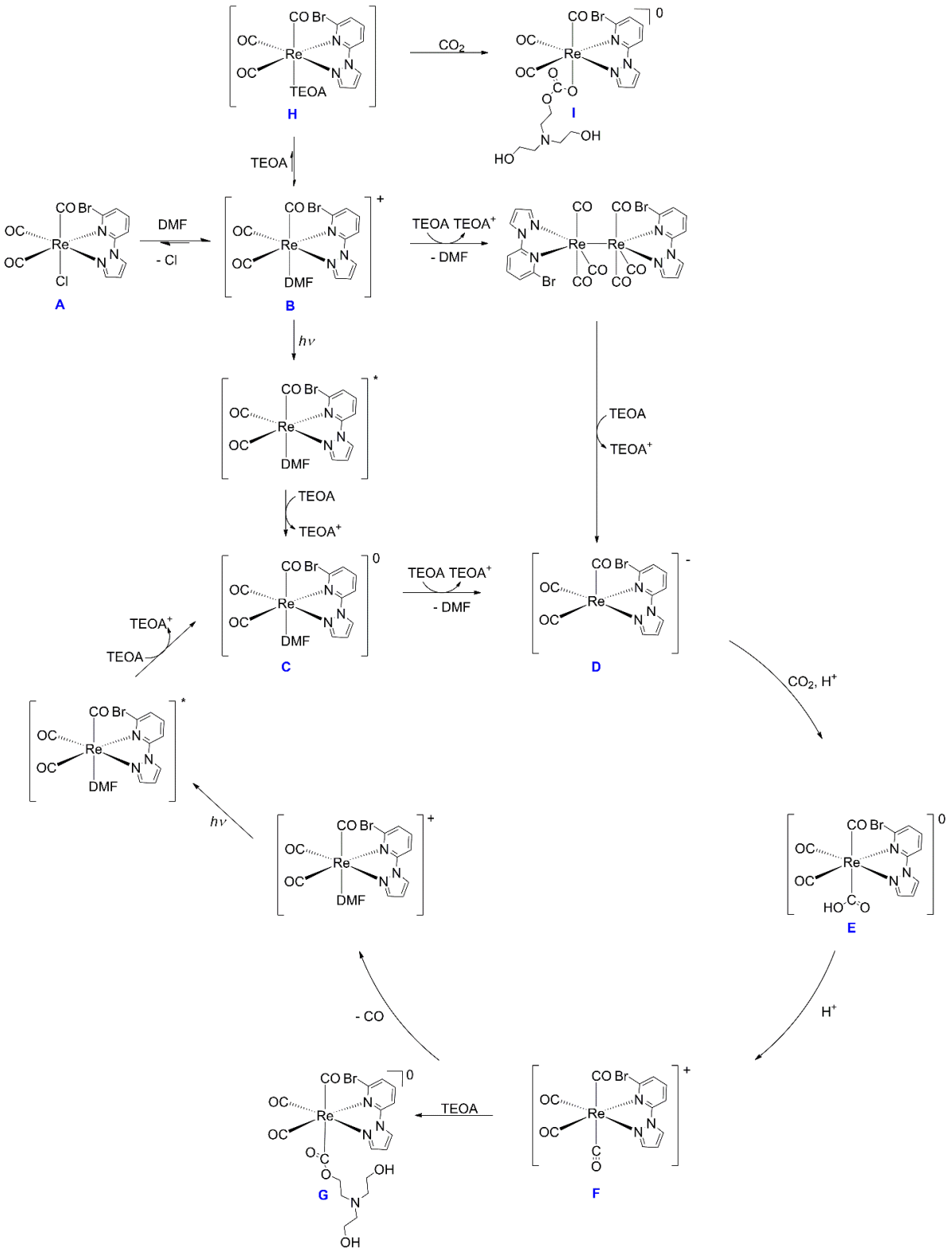

Figure 7: Proposed mechanism for the photochemical reduction of CO_2 to CO catalyzed by **1**.

CONCLUSIONS

In this work we employed a ligand functionalization approach, resulting in the synthesis and characterization of a novel Re(I) complex as a catalyst for CO_2 photoreduction. This complex, formulated as [Re**L1**$(CO)_3$Cl], where **L1**=2-Bromo-6-(1*H*-pyrazol-1-yl)pyridine, exhibited impressive activity even at nanomolar concentrations. The study confirmed the facial octahedral geometry of the rhenium complex and highlighted the importance of DMF coordination during the CO_2 photoreduction process. While this latter process is endergonic by 10.8 kcal mol^{-1}, NMR measurements show that minute quantities are formed which facilitate the subsequent ligand exchange needed for the mechanism.

The redox behavior of **1** indicated a CO_2 reduction mechanism facilitated by CO_2 protonation. This was substantiated through the detection of various species, including [$Re(CO)_3Cl(COOH)$], TEOA−CO_2, and TEOA−CO, utilizing a suite of complementary analytical methods such as NMR, FTIR, and ESI-MS. A remarkable aspect of this novel catalyst is its ability to achieve superior TON_{CO} values of 1517 within a three-hour span at the nanomolar scale under controlled conditions. This performance contrasts with that of previously reported Re(I) catalysts.

Interestingly, ESI-MS analysis has revealed the hitherto undiscovered side product (**G**) exhibiting a Re(I)-CO_2R bond, bearing an organic carbonite functional group. This formation is practically barrierless (+3.2 kcal mol^{-1}) and highly exergonic (-29.0 kcal mol^{-1}).

Addition of CO_2 to the [$Re(CO)_3$(TEOA)] intermediate is also reversible but slow with a 16.8 kcal mol^{-1} barrier height.

The innovative approach to catalyst design presented here holds promise for the development of better photocatalysts for the conversion of pollutants into valuable starting materials, underscoring

the potential for significant impact in the realm of environmental remediation and resource conservation.

ASSOCIATED CONTENT

Experimental details, characterization of the catalyst (^{1}H NMR spectra,^{13}C NMR spectra, FTIR spectrum, UV-vis spectra, Emission spectra, cyclic voltammetry, SCRX data and tables) spectroscopic monitoring of photocatalytic reactions, and in situ generated intermediates by ESI-MS. Atomic coordinates of the computational runs are available in the supporting documents section and online at the iochem-bd repository under the DOI identifier: xxxxx.[75]

AUTHOR INFORMATION

Corresponding Author

*Paulo Nuno Martinho - Centro de Química Estrutural, Institute of Molecular Sciences, Departamento de Química e Bioquímica, Faculdade de Ciências, Universidade de Lisboa, Campo Grande, 1749-016 Lisboa, Portugal; https://orcid.org/0000-0003-2552-6263; pnmartinho@ciencias.ulisboa.pt

Author Contributions

The manuscript was written through contributions of all authors. All authors have given approval to the final version of the manuscript.

ACKNOWLEDGEMENT

Centro de Química Estrutural (CQE) and Institute of Molecular Sciences (IMS) acknowledge the financial support of Fundação para a Ciência e Tecnologia (Projects UIDB/00100/2020, UIDP/00100/2020, and LA/P/0056/2020, respectively). BioISI acknowledges FCT for financial

support (UIDB/04046/2020, UIDP/04046/2020). Paulo N. Martinho thanks FCT for financial support (grant PTDCQUI-QIN0252_2021 and contract CEECIND/00509/2017). S. R. thanks FCT for the contract 2020.02134.CEECIND. M.A.B. thanks FCT for the PhD scholarship (2021.07918.BD). E.J.D. thanks Richard van de Sanden from DIFFER for support and fruitful discussions. H.N.M would like to thank EPSRC (EP/R01308X/1) and the University of Glasgow for supporting this work and Prof. L. Cronin for providing access to the ESI-MS instrumentation. LAQV-REQUIMTE acknowledges FCT-MCTES for financial support (UIDB/50006/2020 and UIDP/50006/2020). COST Actions CA21101 (COSY), CA21127 (TrANsMIT) and CA22131 (LUCES) are also acknowledged.

REFERENCES

(1) Friedlingstein, P.; O'sullivan, M.; Jones, M. W.; Andrew, R. M.; Gregor, L.; Hauck, J.; Le Quéré, C.; Luijkx, I. T.; Olsen, A.; Peters, G. P.; Peters, W.; Pongratz, J.; Schwingshackl, C.; Sitch, S.; Canadell, J. G.; Ciais, P.; Jackson, R. B.; Alin, S. R.; Alkama, R.; Arneth, A.; Arora, V. K.; Bates, N. R.; Becker, M.; Bellouin, N.; Bittig, H. C.; Bopp, L.; Chevallier, F.; Chini, L. P.; Cronin, M.; Evans, W.; Falk, S.; Feely, R. A.; Gasser, T.; Gehlen, M.; Gkritzalis, T.; Gloege, L.; Grassi, G.; Gruber, N.; Gürses, Ö.; Harris, I.; Hefner, M.; Houghton, R. A.; Hurtt, G. C.; Iida, Y.; Ilyina, T.; Jain, A. K.; Jersild, A.; Kadono, K.; Kato, E.; Kennedy, D.; Klein Goldewijk, K.; Knauer, J.; Korsbakken, J. I.; Landschützer, P.; Lefèvre, N.; Lindsay, K.; Liu, J.; Liu, Z.; Marland, G.; Mayot, N.; Mcgrath, M. J.; Metzl, N.; Monacci, N. M.; Munro, D. R.; Nakaoka, S. I.; Niwa, Y.; O'brien, K.; Ono, T.; Palmer, P. I.; Pan, N.; Pierrot, D.; Pocock, K.; Poulter, B.; Resplandy, L.; Robertson, E.; Rödenbeck, C.; Rodriguez, C.; Rosan, T. M.; Schwinger, J.; Séférian, R.; Shutler, J. D.; Skjelvan, I.; Steinhoff, T.; Sun, Q.; Sutton, A. J.; Sweeney, C.; Takao, S.; Tanhua, T.; Tans, P. P.; Tian, X.; Tian, H.; Tilbrook, B.; Tsujino, H.; Tubiello, F.; Van Der Werf, G. R.; Walker, A. P.;

Wanninkhof, R.; Whitehead, C.; Willstrand Wranne, A.; Wright, R.; Yuan, W.; Yue, C.; Yue, X.; Zaehle, S.; Zeng, J.; Zheng, B. Global Carbon Budget 2022. *Earth Syst Sci Data.* **2022**, *14* (11), 4811–4900. DOI: 10.5194/essd-14-4811-2022.

(2) Forster, P. M.; Smith, C. J.; Walsh, T.; Lamb, W. F.; Lamboll, R.; Hauser, M.; Ribes, A.; Rosen, D.; Gillett, N.; Palmer, M. D.; Rogelj, J.; von Schuckmann, K.; Seneviratne, S. I.; Trewin, B.; Zhang, X.; Allen, M.; Andrew, R.; Birt, A.; Borger, A.; Boyer, T.; Broersma, J. A.; Cheng, L.; Dentener, F.; Friedlingstein, P.; Gutiérrez, J. M.; Gütschow, J.; Hall, B.; Ishii, M.; Jenkins, S.; Lan, X.; Lee, J.-Y.; Morice, C.; Kadow, C.; Kennedy, J.; Killick, R.; Minx, J. C.; Naik, V.; Peters, G. P.; Pirani, A.; Pongratz, J.; Schleussner, C.-F.; Szopa, S.; Thorne, P.; Rohde, R.; Rojas Corradi, M.; Schumacher, D.; Vose, R.; Zickfeld, K.; Masson-Delmotte, V.; Zhai, P. Indicators of Global Climate Change 2022: Annual Update of Large-Scale Indicators of the State of the Climate System and Human Influence. *Earth Syst Sci Data*. **2023**, *15* (6), 2295–2327. DOI: 10.5194/essd-15-2295-2023.

(3) Wang, Y.; Chen, E.; Tang, J. Insight on Reaction Pathways of Photocatalytic CO_2 Conversion. *ACS Catal*. **2022**, *12* (12), 7300–7316. DOI: 10.1021/acscatal.2c01012.

(4) Artz, J.; Müller, T. E.; Thenert, K.; Kleinekorte, J.; Meys, R.; Sternberg, A.; Bardow, A.; Leitner, W. Sustainable Conversion of Carbon Dioxide: An Integrated Review of Catalysis and Life Cycle Assessment. *Chem. Rev*. **2018**, *118* (2), 434–504. DOI: 10.1021/acs.chemrev.7b00435.

(5) He, J.; Janáky, C. Recent Advances in Solar-Driven Carbon Dioxide Conversion: Expectations versus Reality. *ACS Energy Lett*. **2020**, *5* (6), 1996–2014. DOI: 10.1021/acsenergylett.0c00645.

(6) Nganga, J.; Wolf, L.; Mullick, K.; Reinheimer, E.; Saucedo, C.; Wilson, M.; Grice, K.; Ertem, M.; Angeles-Boza, A. Methane Generation from CO_2 with a Molecular Rhenium Catalyst. *Inorg. Chem.* **2021**, *60* (6), 3572-3584. DOI: 10.1021/acs.inorgchem.0c02579.

(7) Realista, S.; Almeida J. C.; Milheiro S. A.; Bandeira N. A. G.; Alves L. G.; Madeira F.; Calhorda M. J.; Martinho P. N. Co^{II} Cryptates Convert CO_2 into CO and CH_4 under Visible Light. *Chem. Eur. J.* **2019**, *25* (50), 11670 -11679. DOI: 10.1002/chem.201901806.

(8) Parrino, F.; Fidalgo, A.; Palmisano, L.; Ilharco, L. M.; Pagliaro, M.; Ciriminna, R. Polymers of Limonene Oxide and Carbon Dioxide: Polycarbonates of the Solar Economy. *ACS Omega*. **2018**, *3* (5), 4884 – 4890. DOI: 10.1021/acsomega.8b00644.

(9) Rotundo, L.; Grills, D. C.; Gobetto, R.; Priola, E.; Nervi, C.; Polyansky, D. E.; Fujita, E. Photochemical CO_2 Reduction Using Rhenium(I) Tricarbonyl Complexes with Bipyridyl-Type Ligands with and without Second Coordination Sphere Effects. *ChemPhotoChem*. **2021**, *5* (6), 526–537. DOI:10.1002/cptc.202000307.

(10) Himeda Y.; Onozawa-Komatsuzaki N.; Sugihara H.; Kasuga K. Recyclable Catalyst for Conversion of Carbon Dioxide into Formate Attributable to an Oxyanion on the Catalyst Ligand. *J. Am. Chem. Soc*. **2005**, *127* (38) 13118–13119. DOI: 10.1021/ja054236k.

(11) Takeda, H.; Koike, K.; Inoue, H.; Ishitani, O. Development of an Efficient Photocatalytic System for CO_2 Reduction Using Rhenium(I) Complexes Based on Mechanistic Studies. *J. Am. Chem. Soc*. **2008**, *130* (6), 2023–2031. DOI:10.1021/ja077752e.

(12) Kumar, B.; Llorente, M.; Froehlich, J.; Dang, T.; Sathrum, A.; Kubiak, C. P. Photochemical and Photoelectrochemical Reduction of CO_2. *Annu. Rev. Phys. Chem*. **2012**, *63* (1), 541–569. DOI: 10.1146/annurev-physchem-032511-143759.

(13) Yamazaki, Y.; Takeda, H.; Ishitani, O. Photocatalytic Reduction of CO_2 Using Metal Complexes. *Journal of Photochemistry and Photobiology C: Photochemistry Reviews*. **2015**, *25*, 106–137. DOI:10.1016/j.jphotochemrev.2015.09.001.

(14) Hawecker, J.; Lehn, J. -M; Ziessel, R. Photochemical and Electrochemical Reduction of Carbon Dioxide to Carbon Monoxide Mediated by (2,2′-Bipyridine)Tricarbonylchlororhenium(I) and Related Complexes as Homogeneous Catalysts. *Helv. Chim. Acta.* **1986**, *69* (8), 1990–2012. DOI: 10.1002/hlca.19860690824.

(15) Frayne, L.; Das, N.; Paul, A.; Amirjalayer, S.; Buma, W. J.; Woutersen, S.; Long, C.; Vos, J. G.; Pryce, M. T. Photo- and Electrochemical Properties of a CO_2 Reducing Ruthenium–Rhenium Quaterpyridine-Based Catalyst. *ChemPhotoChem*. **2018**, *2* (3), 323–331. DOI:10.1002/cptc.201700197.

(16) Gholamkhass, B.; Mametsuka, H.; Koike, K.; Tanabe, T.; Furue, M.; Ishitani, O. Architecture of Supramolecular Metal Complexes for Photocatalytic CO_2 Reduction: Ruthenium-Rhenium Bi- and Tetranuclear Complexes. *Inorg. Chem.* **2005**, *44* (7), 2326–2336. DOI:10.1021/ic048779r.

(17) Gotico, P.; Tran, T. T.; Baron, A.; Vauzeilles, B.; Lefumeux, C.; Ha-Thi, M. H.; Pino, T.; Halime, Z.; Quaranta, A.; Leibl, W.; Aukauloo, A. Tracking Charge Accumulation in a Functional Triazole-Linked Ruthenium-Rhenium Dyad Towards Photocatalytic Carbon Dioxide Reduction. *ChemPhotoChem*. **2021**, *5* (7), 654–664. DOI:10.1002/cptc.202100010.

(18) Liyanage, N. P.; Yang, W.; Guertin, S.; Sinha Roy, S.; Carpenter, C. A.; Adams, R. E.; Schmehl, R. H.; Delcamp, J. H.; Jurss, J. W. Photochemical CO_2 Reduction with Mononuclear and Dinuclear Rhenium Catalysts Bearing a Pendant Anthracene Chromophore. *Chem. Commun*. **2019**, *55* (7), 993–996. DOI:10.1039/c8cc09155b.

(19) Giereth, R.; Lang, P.; McQueen, E.; Meißner, X.; Braun-Cula, B.; Marchfelder, C.; Obermeier, M.; Schwalbe, M.; Tschierlei, S. Elucidation of Cooperativity in CO_2 Reduction Using a Xanthene-Bridged Bimetallic Rhenium(I) Complex. *ACS Catal*. **2021**, *11* (1), 390–403. DOI:10.1021/acscatal.0c04314.

(20) Wang, F.; Neumann, R.; De Graaf, C.; Poblet, J. M. Photoreduction Mechanism of CO_2 to CO Catalyzed by a Three-Component Hybrid Construct with a Bimetallic Rhenium Catalyst. *ACS Catal.* **2021**, *11* (3), 1495–1504. DOI:10.1021/acscatal.0c04366.

(21) Kuramochi, Y.; Ishitani, O.; Ishida, H. Reaction Mechanisms of Catalytic Photochemical CO_2 Reduction Using Re(I) and Ru(II) Complexes. *Coordination Chemistry Reviews*. **2018**, *373*, 333–356. DOI:10.1016/j.ccr.2017.11.023.

(22) Müller, A. V.; Faustino, L. A.; De Oliveira, K. T.; Patrocinio, A. O. T.; Polo, A. S. Visible-Light-Driven Photocatalytic CO_2 Reduction by Re(I) Photocatalysts with N-Heterocyclic Substituents. *ACS Catal.* **2023**, *13* (1), 633–646. DOI:10.1021/acscatal.2c05521.

(23) Kuramochi, Y.; Satake, A. Photocatalytic CO_2 Reductions Catalyzed by Meso-(1,10-Phenanthrolin-2-yl)-Porphyrins Having a Rhenium(I) Tricarbonyl Complex. *Chem. Eur. J*. **2020**, *26* (69), 16365–16373. DOI:10.1002/chem.202002558.

(24) Tsubaki H., Sekine A., Ohashi Y., Koike K., Takeda H., and Ishitani O. Control of Photochemical, Photophysical, Electrochemical, and Photocatalytic Properties of Rhenium(I) Complexes Using Intramolecular Weak Interactions between Ligands. *J. Am. Chem. Soc*. **2005**, *127* (44), 15544–15555. DOI: 10.1021/ja053814u.

(25) Asai, Y.; Katsuragi, H.; Kita, K.; Tsubomura, T.; Yamazaki, Y. Photocatalytic CO_2 Reduction Using Metal Complexes in Various Ionic Liquids. *Dalton Trans*. **2020**, *49* (14), 4277–4292. DOI:10.1039/c9dt04689e.

(26) Chen, K. H.; Wang, N.; Yang, Z. W.; Xia, S. M.; He, L. N. Tuning of Ionic Second Coordination Sphere in Evolved Rhenium Catalyst for Efficient Visible-Light-Driven CO_2 Reduction. *ChemSusChem*. **2020**, *13* (23), 6284–6289. DOI:10.1002/cssc.202000698.

(27) Ching, H. Y. V.; Wang, X.; He, M.; Perujo Holland, N.; Guillot, R.; Slim, C.; Griveau, S.; Bertrand, H. C.; Policar, C.; Bedioui, F.; Fontecave, M. Rhenium Complexes Based on 2-Pyridyl-1,2,3-Triazole Ligands: A New Class of CO_2 Reduction Catalysts. *Inorg. Chem.* **2017**, *56* (5), 2966–2976. DOI:10.1021/acs.inorgchem.6b03078.

(28) Koenig, J. D. B.; Piers, W. E.; Welch, G. C. Promoting Photocatalytic CO_2 reduction through Facile Electronic Modification of N-Annulated Perylene Diimide Rhenium Bipyridine Dyads. *Chem. Sci.* **2022**, *13* (4), 1049–1059. DOI:10.1039/d1sc05465a.

(29) Maurin, A.; Ng, C. O.; Chen, L.; Lau, T. C.; Robert, M.; Ko, C. C. Photochemical and Electrochemical Catalytic Reduction of CO_2 with NHC-Containing Dicarbonyl Rhenium(I) Bipyridine Complexes. *Dalton Trans*. **2016**, *45* (37), 14524–14529. DOI:10.1039/c6dt01686c.

(30) Qiu, L. Q.; Yang, Z. W.; Yao, X.; Li, X. Y.; He, L. N. Highly Robust Rhenium(I) Bipyridyl Complexes Containing Dipyrromethene-BF_2 Chromophores for Visible Light-Driven CO_2 Reduction. *ChemSusChem*. **2022**, *15* (14), e202200337. DOI:10.1002/cssc.202200337.

(31) Takeda, H.; Koike, K.; Morimoto, T.; Inumaru, H.; Ishitani, O. Photochemistry and Photocatalysis of Rhenium(I) Diimine Complexes. *Advances in Inorganic Chemistry*, **2011**, *63*, 137-186. DOI:10.1016/B978-0-12-385904-4.00007-X.

(32) Armarego, W. L. F.; Perrin, D. D. *Purification of Laboratory Chemicals,* 4th ed.; Butterworth Heinemann, Elsevier, 1997. ISBN 0 7506 3761 7.

(33) Gong, D.; Liu, W.; Chen, T.; Chen, Z. R.; Huang, K. W. Ethylene Polymerization by PN^3-Type Pincer Chromium(III) Complexes. *J. Mol. Catal. A Chem.* **2014**, *395*, 100–107. DOI:10.1016/j.molcata.2014.08.005.

(34) Sheldrick G. M., A short history of SHELX. *Acta Crystallographica Section A.* **2008**, *64*, 112-122. DOI: 10.1107/S0108767307043930.

(35) Macrae C. F.; Sovago I.; Cottrell S. J.; Galek P. T. A.; McCabe P.; Pidcock E.; Platings M.; Shields G. P.; Stevens J. S.; Towler M.; Wood P. A. Mercury 4.0: from visualization to analysis, design, and prediction. *J. Appl. Cryst*. **2020**, *53*, 226-235. DOI: 10.1107/S1600576719014092.

(36) Neese, F. Software update: The ORCA program system—Version 5.0. *WIREs Comput. Mol. Sci.* **2022**, *12* (5), e1606. DOI: 10.1002/wcms.1606.

(37) Adamo, C.; Barone, V. Toward chemical accuracy in the computation of NMR shieldings: the PBE0 model. *Chem. Phys. Lett.* **1998,** *298* (1–3), 113-119. DOI: 10.1016/S0009-2614(98)01201-9.

(38) Adamo, C.; Barone, V. Toward reliable density functional methods without adjustable parameters: The PBE0 model. *J. Chem. Phys.* **1999,** *110* (13), 6158-6170. DOI:10.1063/1.478522.

(39) Caldeweyher, E.; Bannwarth, C.; Grimme, S. Extension of the D3 dispersion coefficient model. *J. Chem. Phys.* **2017,** *147* (3), 034112. DOI: 10.1063/1.4993215.

(40) Pollak, P.; Weigend, F. Segmented Contracted Error-Consistent Basis Sets of Double- and Triple-ζ Valence Quality for One- and Two-Component Relativistic All-Electron Calculations. *J. Chem. Theory Comput.* **2017,** *13* (8), 3696-3705. DOI: 10.1021/acs.jctc.7b00593.

(41) Dyall, K. G.; van Lenthe, E. Relativistic regular approximations revisited: An infinite-order relativistic approximation. *J. Chem. Phys.* **1999,** *111* (4), 1366-1372. DOI: 10.1063/1.479395.

(42) Helmich-Paris, B.; Souza, B. d.; Neese, F.; Izsák, R. An improved chain of spheres for exchange algorithm. *J. Chem. Phys.* **2021,** *155* (10), 104109. DOI: 10.1063/5.0058766.

(43) Neese, F. The SHARK integral generation and digestion system. *J. Comput. Chem.* **2022**, *44* (3), 381-396. DOI: 10.1002/jcc.26942.

(44) Barone, V.; Cossi, M.. Quantum Calculation of Molecular Energies and Energy Gradients in Solution by a Conductor Solvent Model. *J. Phys. Chem. A* **1998,** *102* (11), 1995-2001. DOI: 10.1021/jp9716997.

(45) Cammi, R.; Mennucci, B.; Tomasi, J. Fast Evaluation of Geometries and Properties of Excited Molecules in Solution: A Tamm-Dancoff Model with Application to 4-

Dimethylaminobenzonitrile. *J. Phys. Chem. A* **2000,** *104* (23), 5631-5637. DOI: 10.1021/jp000156l.

(46) Lu, T.; Chen, F. Multiwfn: A Multifunctional Wavefunction Analyzer. *J. Comput. Chem.* **2012,** *33* (5), 580-592. DOI: 10.1002/jcc.22885.

(47) de Souza, B.; Neese, F.; Izsák, R. On the Theoretical Prediction of Fluorescence Rates From First Principles Using the Path Integral Approach. *J. Chem. Phys.* **2018,** *148* (3), 034104. DOI: 10.1063/1.5010895.

(48) Kumagai, H.; Nishikawa, T.; Koizumi, H.; Yatsu, T.; Sahara, G.; Yamazaki, Y.; Tamaki, Y.; Ishitani, O. Electrocatalytic Reduction of Low Concentration CO_2. *Chem. Sci*. **2019**, *10* (6), 1597–1606. DOI:10.1039/c8sc04124e.

(49) Rohacova, J.; Ishitani, O. Photofunctional Multinuclear Rhenium(I) Diimine Carbonyl Complexes. *Dalton Trans*. **2017**, *46*, 8899–8919. DOI:10.1039/c7dt00577f.

(50) Koizumi, H.; Chiba, H.; Sugihara, A.; Iwamura, M.; Nozaki, K.; Ishitani, O. CO_2 Capture by Mn(I) and Re(I) Complexes with a Deprotonated Triethanolamine Ligand. *Chem. Sci*. **2019**, *10* (10), 3080–3088. DOI:10.1039/c8sc04389b.

(51) Morimoto, T.; Nakajima, T.; Sawa, S.; Nakanishi, R.; Imori, D.; Ishitani, O. CO_2 Capture by a Rhenium(I) Complex with the Aid of Triethanolamine. *J. Am. Chem. Soc.* **2013**, *135* (45), 16825–16828. DOI:10.1021/ja409271s.

(52) Ci, C.; Carbó, J. J.; Neumann, R.; Graaf, C. De; Poblet, J. M. Photoreduction Mechanism of CO_2 to CO Catalyzed by a Rhenium(I)-Polyoxometalate Hybrid Compound. *ACS Catal*. **2016**, *6* (10), 6422–6428. DOI:10.1021/acscatal.6b01638.

(53) Rodríguez, L.; Ferrer, M.; Rossell, O.; Duarte, F. J. S.; Gil Santos, A.; Lima, J. C. Solvent Effects on the Absorption and Emission of [Re(R_2bpy)$(CO)_3$X] Complexes and Their Sensitivity to CO_2 in Solution. *J. Photochem. Photobiol. A Chem*. **2009**, *204* (2–3), 174–182. DOI:10.1016/j.jphotochem.2009.03.022.

(54) Heß, B. A.; Marian, C. M.; Wahlgren, U.; Gropen, O. A Mean-Field Spin-Orbit Method Applicable to Correlated Wavefunctions. *Chem. Phys. Lett.* **1996**, *251* (5-6), 365-371. DOI: 10.1016/0009-2614(96)00119-4.

(55) Spear, A.; Schuarca, R. L.; Bond, J. Q.; Korter, T. M.; Zubieta, J.; Doyle, R. P. Photocatalytic Turnover of CO_2 under Visible Light by [Re$(CO)_3$(1-(1,10) Phenanthroline-5-(4-Nitro-Naphthalimide))Cl] in Tandem with the Sacrificial Donor BIH. *RSC Adv*. **2022**, *12* (9), 5080–5084. DOI:10.1039/d1ra08261b.

(56) Machan, C. W.; Chabolla, S. A.; Yin, J.; Gilson, M. K.; Tezcan, F. A.; Kubiak, C. P. Supramolecular Assembly Promotes the Electrocatalytic Reduction of Carbon Dioxide by Re(I) Bipyridine Catalysts at a Lower Overpotential. *J. Am. Chem. Soc.* **2014**, *136* (41), 14598–14607. DOI:10.1021/ja5085282.

(57) Kutal, C.; Corbin, J.; Ferraudi, G. Further Studies of the Photoinduced Reduction of Carbon Dioxide Mediated by Tricarbonylbromo (2,2'-Bipyridine) Rhenium (I). *Organometallics*. **1987**, *6* (3), 553–557. DOI:10.1021/om00146a020

(58) Kutal, C.; Weber, M. A.; Ferraudi, G.; Geiger, D. A Mechanistic Investigation of the Photoinduced Reduction of Carbon Dioxide Mediated by Tricarbonylbromo (2,2'-Bipyridine)Rhenium(I), *Organometallics*, **1985**, *4* (12), 2161–2166. DOI: 10.1021/om00131a016.

(59) Johnson, F. P. A.; George, M. W.; Hartl, F.; Turner, J. J. Electrocatalytic Reduction of CO_2 Using the Complexes $[Re(bpy)(CO)_3L]^n$ (n = +1, L = $P(OEt)_3$, CH_3CN; n = 0, L = Cl^-, Otf^-; bpy = 2,2′-Bipyridine; Otf^- = CF_3SO_3) as Catalyst Precursors: Infrared Spectroelectrochemical Investigation. *Organometallics*. **1996**, *15* (15), 3374–3387. DOI: 10.1021/om960044.

(60) Sampson, M. D.; Froehlich, J. D.; Smieja, J. M.; Benson, E. E.; Sharp, I. D.; Kubiak, C. P. Direct Observation of the Reduction of Carbon Dioxide by Rhenium Bipyridine Catalysts. *Energy Environ. Sci*. **2013**, *6* (12), 3748–3755. DOI:10.1039/c3ee42186d.

(61) Qiu, L. Q.; Chen, K. H.; Yang, Z. W.; Ren, F. Y.; He, L. N. Prolonging the Triplet State Lifetimes of Rhenium Complexes with Imidazole-Pyridine Framework for Efficient CO_2 Photoreduction. *Chem. Eur. J*. **2021**, *27* (62), 15536. DOI:10.1002/chem.202102837.

(62) Benson, E. E.; Kubiak, C. P. Structural Investigations into the Deactivation Pathway of the CO_2 Reduction Electrocatalyst $Re(bpy)(CO)_3Cl$. *Chem. Comm*. **2012**, *48* (59), 7374–7376. DOI:10.1039/c2cc32617e.

(63) Miras, H. N.; Sorus, M.; Hawkett, J.; Sells, D. O.; McInnes, E. L.; Cronin, L. Oscillatory Template Exchange in Polyoxometalate Capsules: A Ligand-Triggered, Redox-Powered, Chemically Damped Oscillation. *J. Am. Chem. Soc.* **2012**, *134*, 6980-6983. DOI: 10.1021/ja302861z.

(64) Miras, H. N.; Wilson, E. F.; Cronin, L. Unravelling the Complexities of Inorganic and Supramolecular Self-Assembly in Solution With Electrospray and Cryospray Mass Spectrometry. *Chem. Commun.* **2009**, *11*, 1297-1311. DOI: 10.1039/B819534J.

(65) Kou, Y.; Nabetani, Y.; Masui, D.; Shimada, T.; Takagi, S.; Tachibana, H.; Inoue, H. Direct Detection of Key Reaction Intermediates in Photochemical CO_2 Reduction Sensitized by a Rhenium Bipyridine Complex. *J. Am. Chem. Soc*. **2014**, *136* (16), 6021–6030. DOI:10.1021/ja500403e.

(66) Kou, Y.; Nabetani, Y.; Nakazato, R.; Pratheesh, N. V.; Sato, T.; Nozawa, S.; Adachi, S. ichi; Tachibana, H.; Inoue, H. Mechanism of the Photoreduction of Carbon Dioxide Catalyzed by the Benchmarking Rhenium Dimethylbipyridine Complexes; Operando Measurements by XAFS and FT-IR. *J. Catal*. **2022**, *405*, 508–519. DOI:10.1016/j.jcat.2021.11.020.

(67) Chabolla, S. A.; Machan, C. W.; Yin, J.; Dellamary, E. A.; Sahu, S.; Gianneschi, N. C.; Gilson, M. K.; Tezcan, F. A.; Kubiak, C. P. Bio-Inspired CO_2 Reduction by a Rhenium Tricarbonyl Bipyridine-Based Catalyst Appended to Amino Acids and Peptidic Platforms: Incorporating Proton Relays and Hydrogen-Bonding Functional Groups. *Faraday Discuss.* **2017**, *198*, 279–300. DOI:10.1039/c7fd00003k.

(68) Miras, H. N.; Long, D. L.; Kögerler, P.; Cronin, L. Bridging the Gap Between Solution and Solid-State Studies in Polyoxometalate Chemistry: Discovery of a Family Of $[V_1M_{17}]$-Based Cages Encapsulating Two $\{(VO_4)$-O-V$\}$ Moieties. *Dalton Trans.* **2008**, *52*, 214-221. DOI: 10.1039/B714285D.

(69) Miras, H. N.; Stone, D.; Long, D. L.; McInnes, E. L.; Kögerler, P.; Cronin, L. Exploring the Structure and Properties of Transition Metal Templated $\{VM_{17}(VO_4)_2\}$ Dawson-Like Capsules. *Inorg. Chem.* **2011**, *50* (17), 8384–839. DOI: 10.1021/ic200943s.

(70) Zang, H. Y.; Chen, J. J.; Long, D. L.; Cronin, L.; Miras, H. N. Assembly of Thiometalate-Based $\{Mo_{16}\}$ and $\{Mo_{36}\}$ Composite Clusters Combining $[Mo_2O_2S_2]^{2+}$ Cations and Selenite Anions. *Adv. Mater.* **2013**, *25*, 6245-6249. DOI: 10.1002/adma.201302565.

(71) Yan, J.; Long, D. L.; Miras, H. N.; Cronin, L. Cation Controlled Assembly and Transformation of Mono- and Bi-Sulfite Templated Dawson-Type Polyoxotungstates. *Inorg. Chem.* **2010**, *49*, 1819-1825. DOI: 10.1021/ic9021646.

(72) Hayashi, Y.; Kita, S.; Brunschwig, B. S.; Fujita, E. Involvement of a Binuclear Species with the Re-C(O)O-Re Moiety in CO_2 Reduction Catalyzed by Tricarbonyl Rhenium(I) Complexes with Diimine Ligands: Strikingly Slow Formation of the Re-Re and Re-C(O)O-Re Species from $Re(Dmb)(CO)_3S$ (Dmb = 4,4′-Dimethyl-2,2′-Bipyridine, S = Solvent). *J Am. Chem. Soc*. **2003**, *125* (39), 11976–11987. DOI:10.1021/ja035960a.

(73) George, M. W.; Johnson, F. P. A.; Westwell, J. R.; Hodges, P. M.; Turner, J. J. Excited-State Properties and Reactivity of [ReCl(CO)(2,2'-bipy)] (2,2'-Bipy = 2,2'-bipyridyl) Studied by Time-Resolved Infrared Spectroscopy. *J. Chem. Soc*. *Dalton Trans.* **1993**, *19*, 2977-2979. DOI: 10.1039/DT9930002977.

(74) Cannizzo, A.; Blanco-Rodríguez, A. M.; El Nahhas, A.; Šebera, J.; Záliš, S.; Vlček, A., Jr.; Chergui, M. Femtosecond Fluorescence and Intersystem Crossing in Rhenium(I) Carbonyl−Bipyridine Complexes. *J. Am. Chem. Soc.* **2008**, *130* (28), 8967-8974. DOI: 10.1021/ja710763w.

(75) Álvarez-Moreno M., Graaf C. de, López N., Maseras F., Poblet J. M., and Bo C. Managing the Computational Chemistry Big Data Problem: The ioChem-BD Platform. *J. Chem. Inf. Model*. **2015**, *55* (1), 95–103. DOI: 10.1021/ci500593j.